Title

The Arabidopsis INNER NO OUTER (INO) gene acts exclusively and quantitatively in regulation of ovule outer integument development

Journal

Plant Direct, 7(2)

ISSN

2475-4455

Authors

Skinner, Debra J
Dang, Trang
Gasser, Charles S

Publication Date

2023-02-01

DOI

10.1002/pld3.485

Peer reviewed

Received: 15 August 2022 | Revised: 9 January 2023 | Accepted: 6 February 2023

DOI: 10.1002/pld3.485

ORIGINAL RESEARCH

The Arabidopsis *INNER NO OUTER* (*INO*) gene acts exclusively and quantitatively in regulation of ovule outer integument development

Debra J. Skinner | **Trang Dang** | **Charles S. Gasser**

Dept. of Molecular and Cellular Biology, University of California—Davis, Davis, California, USA

Correspondence
Charles S. Gasser, Dept. of Molecular and Cellular Biology, University of California—Davis, Davis, CA 95616 USA.
Email: csgasser@ucdavis.edu

Present addresses
Debra J. Skinner, Dept. of Plant Biology, University of California—Davis, Davis, California, USA; and Trang Dang, Lark Seeds International, Davis, California, USA.

Funding information
This work was supported in part by the US National Science Foundation grant IOS1354014 (to CSG).

Abstract

The *INNER NO OUTER* (*INO*) gene is essential for formation of the outer integument of ovules in *Arabidopsis thaliana*. Initially described lesions in *INO* were missense mutations resulting in aberrant mRNA splicing. To determine the null mutant phenotype, we generated frameshift mutations and found, in confirmation of results on another recently identified frameshift mutation, that such mutants have a phenotype identical to the most severe splicing mutant (*ino-1*), with effects specific to outer integument development. We show that the altered protein of an *ino* mRNA splicing mutant with a less severe phenotype (*ino-4*) does not have *INO* activity, and the mutant is partial because it produces a small amount of correctly spliced *INO* mRNA. Screening for suppressors of *ino-4* in a fast neutron-mutagenized population identified a translocated duplication of the *ino-4* gene, leading to an increase in the amount of this mRNA. The increased expression led to a decrease in the severity of the mutant effects, indicating that the amount of *INO* activity quantitatively regulates outer integument growth. The results further confirm that the role of *INO* in Arabidopsis development is specific to the outer integument of ovules where it quantitatively affects the growth of this structure.

KEYWORDS
fast neutron mutagenesis, *INNER NO OUTER*, integument, ovule, suppressor mutant, translocation

1 | INTRODUCTION

As the structures that develop into seeds, ovules are an essential component of sexual reproduction in seed plants. Angiosperm ovules comprise a combination of diploid maternal tissues and the haploid megagametophyte that develops to form the embryo and endosperm following double fertilization. Most angiosperm ovules include two sheathing maternal structures, the integuments, which appear to be essential for aspects of fertilization and/or embryo development and that further develop themselves, forming the seed coat. Genes involved in regulation of integument formation have been described in *Arabidopsis thaliana* through mutant and molecular studies, with many found to encode transcription factors. While having important roles in other aspects of plant development, the *AINTEGUMENTA* (*ANT*) and *WUSCHEL* (*WUS*) genes are necessary for integument formation, with mutation in either gene, leading to a complete absence of integuments (Baker et al., 1997; Gross-Hardt et al., 2007; Modrusan et al., 1994). The pattern of *WUS* expression is regulated by *NOZZLE/SPOROCYTELES* (*NZZ/SPL*) (Sieber et al., 2004). Integument identity is under the control of *BELL1* (*BEL1*) (Modrusan et al., 1994;

Ray et al., 1994; Reiser et al., 1995; Robinson-Beers et al., 1992) and a combination of the MADS-box genes *SEEDSTICK* (*STK*) and *SHATTERPROOF 1* and *2* (*SHP1* and *SHP2*) with mutations leading to formation of amorphous or carpelloid structures in place of integuments (Pinyopich et al., 2003). Determinants of polarity also play roles in development of the bifacial integuments. Adaxial polarity determinants such as members of the Class III HDZIP family play important roles in the final shapes of the two integuments (Kelley et al., 2009). Two KANADI (KAN) genes, *KAN1* and *KAN2*, are abaxial determinants necessary for planar extension of the outer integument (OI) (Eshed et al., 2001; McAbee et al., 2006), and *ABERRANT TESTA SHAPE* (*ATS/KAN4*) partners with *ETTIN/ARF3* to regulate inner integument (II) extension and integument separation (Kelley et al., 2012; McAbee et al., 2006). Only one member of the *YABBY* gene family of abaxial determinants, *INNER NO OUTER* (*INO*), is involved in integument development, and it acts as a master gene in development of the OI with strong *ino* mutants leading to complete absence of this structure (Baker et al., 1997; Vijayan et al., 2021; Villanueva et al., 1999). Genetic and physical interactions between these transcription factors have been studied in many cases (Gasser & Skinner, 2019; Reviewed in Barro-Trastoy et al., 2020).

Arabidopsis ovule morphogenesis has been characterized by scanning electron microscopy, sectioning (Robinson-Beers et al., 1992), clearing (Schneitz et al., 1995), and more recently by elegant confocal and computational analysis (Vijayan et al., 2021). During morphogenesis, the OI, and hence its primary regulator, *INO*, is a major determinant of ovule asymmetry and form. Asymmetric development of the ovule begins with curvature of the funiculus in the direction of the base of the gynoecium (the gynobasal direction) (Figure 1a). The II initiates in a symmetrical ring of cells around the ovule primordium (Figure 1a). *INO* expression and OI development initiate on the gynobasal side of the ovule on the inside of the funicular curve (Robinson-Beers et al., 1992; Vijayan et al., 2021; Villanueva et al., 1999) (Figure 1a). OI development continues with maximal growth on the gynobasal side of the ovule, resulting in curvature of the distal part of the ovule toward the apex of the gynoecium (the gynoapical direction), producing the final "S" shape of the ovule with the micropyle oriented gynoapically (Figure 1b and Figure 2a). Curvature of the embryo sac is driven by cell divisions in a chalazal region internal to the surrounding OI (Figure 1b). In the strong *ino-1* mutant, funicular curvature occurs in the gynobasal direction just as in the wild-type (Figure 1c), but the complete absence of OI initiation or subsequent OI growth leaves the micropyle oriented in the gynobasal direction (Figure 1d and Figure 2b). The proliferation of the chalazal region occurs in *ino-1*, forming a thick collar of tissue below the exposed II (Figure 1d and Figure 2b).

Only two different lesions in the Arabidopsis *INO* locus were identified in extensive forward mutant screens (Baker et al., 1997; Villanueva et al., 1999). Both are single-base substitutions in introns that result in new upstream splice acceptor sites. While being independently isolated, the *ino-1* and *ino-2* alleles have identical substitutions in intron five, creating an *AG* doublet that when utilized as a splicing acceptor site adds 11 bases to the mRNA, leading to a

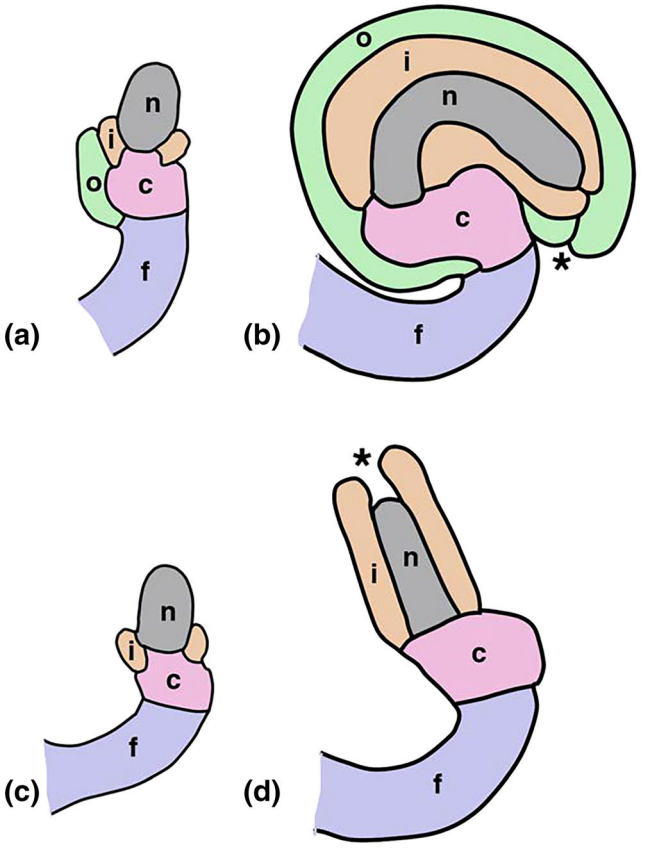

FIGURE 1 Diagrams of ovule sections. A, B wild-type; C, D *ino-1* mutant. All ovules are oriented with the gynoapical side to the right. (a) Wild-type ovule at Stage 2-IV where inner integuments (IIs) and outer integuments (OIs) have been initiated from the chalaza. (b) Wild-type ovule at Stage 3-VI where the OI encloses the II, nucellus, and chalazal region. Asymmetric expansion of the OI places the micropylar opening on the gynoapical side of the ovule. (c) *ino-1* mutant ovule at Stage 2-IV where only the II has initiated from the chalaza. (d) *ino-1* mutant ovule at Stage 3-VI, the II has covered the nucellus, but absence of the OI leaves the micropyle directed toward the gynobasal side of the ovule. Bar in (a) is 50 μm in all panels. Diagrams based on Baker et al. (1997)and Vijayan et al. (2021). Stages from (Schneitz et al., 1995). c, chalaza; f, funiculus; i, inner integument; n, nucellus; o, outer integument; *, micropyle.

frameshift near the start of the essential *YABBY* domain (Villanueva et al., 1999). Absence of the OI in homozygous mutants results in near complete female infertility. That this is a secondary effect of the integument absence is shown by normal segregation of the recessive mutation in heterozygous progeny, where the haploid *ino* mutant embryo sacs effectively produce seed when they form within the wild-type phenotype heterozygous maternal tissue (Baker et al., 1997; Villanueva et al., 1999). Another *ino* allele, *ino-4*, has a substitution in intron four, also introducing an *AG* doublet that acts as a splice acceptor site. In this case, 15 bases are inserted into the mRNA, resulting to addition of five amino acids in the *YABBY* domain of the translation product, while still maintaining the reading frame for the remainder of the protein (Villanueva et al., 1999). *ino-4* has a less severe phenotype than *ino-1* (Villanueva et al., 1999). In *ino-4*, the OI initiates, but OI

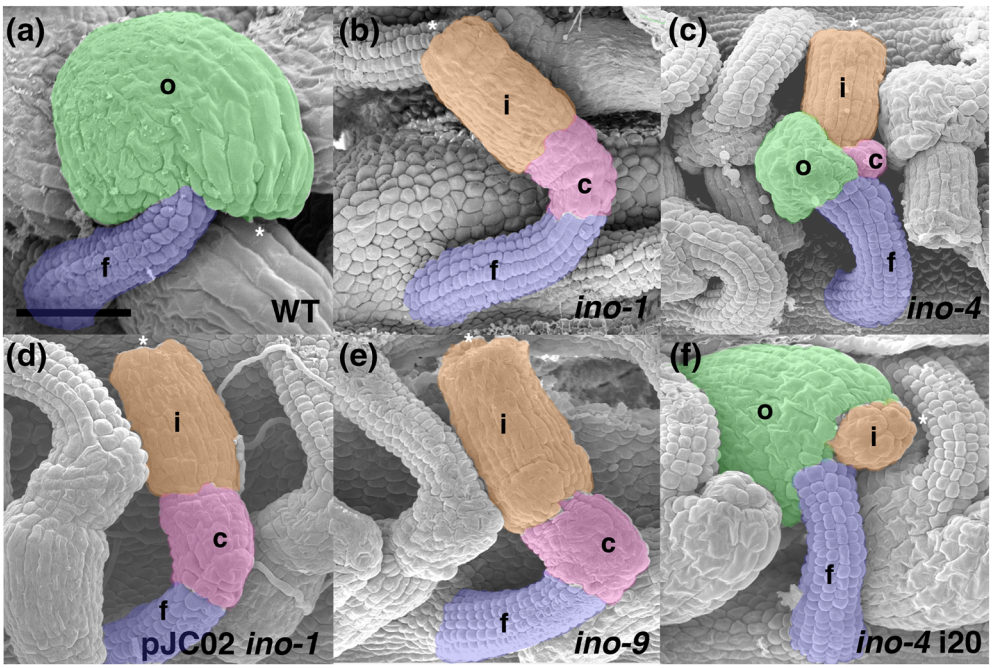

FIGURE 2 Scanning electron micrographs of Arabidopsis ovules. False color has been added to emphasize ovule structures. All ovules are from flowers at or just following anthesis and are oriented with the gynoapical side to the right. (a) Wild-type ovule where the curved outer integument has covered the inner integument. (b) *ino-1* mutant ovule where the outer integument is absent, exposing the inner integument, which remains erect due to this absence, and the chalazal region. (c) *ino-4* mutant ovule has a rudimentary outer integument structure, which fails to cover the inner integument, and from which the expanding chalazal region protrudes. (d) Ovules of *ino-1* mutant plant containing transgene transcribing the mutant *ino-4* cDNA (pJC02) that fails to complement so that the ovules retain the *ino-1* phenotype. (e) *ino-9* mutant ovules that are phenotypically indistinguishable from those of *ino-1*. (f) *i20* partially restores outer integument growth of *ino-4* so that in the *ino-4 i20* double mutant the outer integument can largely cover the inner integument and chalaza, leaving only a small part of the inner integument protruding. Bar in (a) is 50 μm in all panels. c, chalaza; f, funiculus; i, inner integument; o, outer integument; *, micropyle.

development arrests after only a small amount of growth, leaving the II largely exposed (Figure 2c). Chalazal cell proliferation occurs within the abortive OI and sometimes bulges out from this incomplete structure on the gynoapical side (Figure 2c). *ino-4* also produces more seeds that *ino-1* but fewer seeds than the wild-type (Villanueva et al., 1999). The weaker phenotype was hypothesized to be due to partial activity of the *INO* protein with inserted amino acids (Villanueva et al., 1999).

The altered splicing nature of the only two *ino* mutations initially described in Arabidopsis raised several questions. Both described mutations resulted in the introduction of splice acceptor sites that produce aberrant mRNAs. However, both also retain the original splice acceptors, raising the possibility that both could still produce wild-type *INO* mRNA. The assay used to indicate that normal *INO* mRNA was not produced, and direct sequencing of synthesized cDNA (Villanueva et al., 1999) is not especially sensitive, and low levels of wild-type mRNA could have been present. Thus, the actual *ino* null mutant phenotype in Arabidopsis was not clear. It is possible that such a mutation could produce deleterious pleiotropic effects precluding isolation. To assess this, we set out to identify null mutant alleles and used CRISPR (clustered regularly interspaced short palindromic repeats)-mediated mutagenesis to create null mutants. Prior to completion of this manuscript, another group used the same method to identify a putative null mutant, *ino-5*, and showed that it did not have such pleiotropic effects (Vijayan et al., 2021). Another question arising from the nature of the initially identified mutants is whether the *ino-4* weak mutant effect results from a protein with reduced activity or from partial leakage of wild-type mRNA formation in this mutant. Finally, we do not know if levels of INO activity differentially affect OI formation.

To address these questions, we have reexamined the existing *ino* mutants by additional means, have obtained and characterized additional mutants that include likely null mutants, and have isolated a second-site mutant that addresses the question of quantitative expression of *INO*. As also shown in a recent study (Vijayan et al., 2021), we find that newly isolated null mutants duplicate the phenotypic effects of the *ino-1* mutant, indicating that *ino-1* is also effectively a null mutant. We show that the altered protein of *ino-4* does not have *INO* activity, and the phenotype is weak because it produces a small amount of normal *INO* mRNA. A gene duplication leading to a quantitative increase in the amount of this mRNA leads to a decrease in the severity of the effects, indicating that the amount of *INO* activity quantitatively regulates the developmental effects of *INO*. The results further confirm that the role of *INO* in Arabidopsis development is specific to the OI of ovules.

2 | MATERIALS AND METHODS

2.1 | Plant material

Arabidopsis plants were grown under long-day conditions as previously described (McAbee et al., 2006). Preexisting alleles used in this study are *ino-1* (in the L*er* background), *ino-4* (in the Col-0 background) (Villanueva et al., 1999), and *ino-9* (SALK_0063818) (Alonso et al., 2003). Plant transformation utilized *Agrobacterium* GV3101 (Koncz & Schell, 1986) and the floral dip method (Clough & Bent, 1998).

For ovule and seed counts, six fruits were collected after abscission of the other floral organs, starting from the fourth fruit produced. Fruits were collected from at least two different plants for each examined genotype. Aborted ovules and ovules forming seeds were counted in each of the two fruit locules (carpels) using a Zeiss (Oberkochen, Germany) SV8 stereomicroscope. Statistical analysis was performed in GraphPad Prism (San Diego, CA).

2.2 | Plasmid manipulation

pJC02—To clone the cDNA for the aberrantly spliced *ino-4* mRNA, cDNA was synthesized from *ino-4* mRNA using Superscript II reverse transcriptase (RT) and oligo deoxythymidine (dT) primers (Thermo Fisher Scientific, Waltham, MA). The specific cDNA was amplified by polymerase chain reaction (PCR) using Phusion DNA polymerase (New England Biolabs, Ipswich, MA) and primers AtINOcDNA-f and AtINOcDNA-r (Supporting information Table S1), which introduce flanking BamHI and XbaI sites, respectively. The resulting PCR product was inserted into pJet2.1 using the CloneJet cloning kit (Thermo Fisher Scientific, Waltham, MA), and one sequence-verified *ino-4*-specific cDNA clone was designated pSR06. The cDNA in pSR06 was transferred into pJRM42 (a derivative of pRJM33—the expression vector for the wild-type INO cDNA from the wild-type INO promoter; Meister et al., 2005) as a BamH1/Xba1 fragment at these same sites, creating pJC01. pJC01 is identical to pRJM33 except having the ino-4 cDNA replacing the wild-type INO cDNA. The NotI insert fragment of pJC01 containing the complete promoter cDNA expression cassette was inserted into the NotI site of pMLBART (Gleave, 1992) to create the plant transformation vector pJC02, which can be selected in plants for phosphinothricin resistance.

CRISPR mutagenesis—For CRISPR-mediated mutagenesis, we utilized the dual guide RNA approach of Pauwels et al. (2018). Two guide RNA targeting sequences are inserted into two similar vectors at *Bpi*I sites where they are adjacent to Arabidopsis U6 RNA promoters and other constant sequences of the guide RNA, and these two transcription units are subsequently inserted into a plant transformation vector by site-directed recombination using LR Clonase II (Thermo Fisher Scientific, Waltham, MA) (Pauwels et al., 2018). In our case, the synthetic guide RNA targeting sequences INOCRIS4 and INOCRIS5 (Supporting information Table S1) were inserted into the *Bpi*I sites of pMR218 (Pauwels et al., 2018) and a derivative of pMR217 (Pauwels et al., 2018) with a synthetic U6 RNA promoter. LR Clonase II was used to insert the transcription units from these two plasmids into a derivative of plant transformation plasmid pDE-CAS9Km (Pauwels et al., 2018) in which the kanamycin resistance gene is replaced by a gene expressing phosphinothricin acetyltransferase (conferring resistance to BASTA herbicide) and also incorporating a gene for production of the green fluorescent protein (eGFP) in the embryo under control of the Arabidopsis oleosin promoter (Plant et al., 1994), resulting in pGD60. GFP fluorescence in the embryo from the *P-Oleosin::eGFP* gene allows for the differentiation of seeds harboring the CRISPR plasmid from those which have lost the plasmid through genetic segregation (Aliaga-Franco et al., 2019).

2.3 | PCRs

PCRs utilized DreamTaq polymerase (Thermo Fisher Scientific, Waltham, MA) and the supplied reaction buffer components. Superscript II RT (Thermo Fisher Scientific, Waltham, MA) with oligo dT primers was used for cDNA synthesis for reverse transcriptase-polymerase chain reaction (RT-PCR).

2.4 | Microscopy

Scanning electron microscopy was performed as described (Kelley et al., 2009). Dark field images were acquired on a Zeiss Axioplan microscope (Carl Zeiss Inc, Oberkochen, Germany) with a Moticam 5 digital camera (Motic Inc., San Antonio, TX). Images were cropped and matched for contrast in Adobe Photoshop CS5 (Adobe, San Jose, CA).

2.5 | Fast neutron mutagenesis and mutant identification

Homozygous *ino-4* seeds were mutagenized with fast neutrons (60 Gy) at the University of California, Davis McClellan Nuclear Research Center, Sacramento, CA. The treatment resulted in 20%–30% lethality, and 10%–20% of the surviving seed produced fully infertile plants. M1 seeds were planted in pools of five plants. M2 seeds from each pool were collected, and 50 seeds from each pool were planted and grown to anthesis. Ovules were examined under a stereomicroscope to detect deviations from the *ino-4* mutant phenotype.

2.6 | Genetic mapping and whole-genome analysis

To map the location of the mutation responsible for the suppressed *ino*-4 phenotype (*i20*), we outcrossed the *i20/i20 ino-4/ino-4* plants to L*er*. The F2 progeny from this cross were used to map the location of *i20* to Chromosome 3 using Cleaved Amplified Polymorphic

Sequences (CAPS), and Simple Sequence Length Polymorphism (SSLP) markers (Jander et al., 2002) and InDel markers (Hou et al., 2010). The suppressed phenotype observed in the *i20* mutation acted semi-dominantly; thus, individuals used for fine mapping were progeny-tested, and only homozygous individuals were used for further analysis. The mapped location of *i20* was between marker nga126 (3.098 Mb) and 3-4608 (4.608 Mb). A total of 12 individuals from F2 and F3 mapping populations, homozygous for *ino-4* and *i20*, were used to extract DNA for sequencing.

Leaf samples from *ino-4* and *ino-4 i20* plants were separately pooled and DNA was extracted with Nucleon Phytopure DNA extraction kit (GE Healthcare, Pittsburgh, PA), according to the provider's instructions. NEBNext DNA library components (New England Biolabs, Ipswich, MA) were used for fragmentation to 200–500 bp and library preparation with Nextflex-96 indexes (Bioo Scientific, Austin, TX).

Libraries were pooled and sequenced using the PE100 bp protocol on a single lane of Hiseq 2000 (Illumina, Inc., San Diego, CA) at the Vincent J. Coates Genomics Sequencing Laboratory at UC Berkeley. A total of 67.5 and 99.9 million reads were obtained for *ino-4* and *ino-4 i20*, respectively. Reads were preprocessed to remove tag and poor-quality regions using Sickle (Version 1.33, https://github.com/najoshi/sickle) and Scythe (https://github.com/najoshi/scythe), respectively. Reads were aligned with the Col-0 TAIR 10 reference sequence (Lamesch et al., 2012) using BWA-MEM (Li, 2013). Aligned sequences were viewed in Tablet (Milne et al., 2013) to visualize changes relative to the wild-type Col-0 sequence in the region identified as including the *i20* suppressor based on the mapping.

3 | RESULTS

3.1 | *ino-4* mis-spliced mRNA cannot support OI growth

Whereas the *ino-1* mutant exhibits no growth of the OI, the *ino-4* mutant shows partial OI growth ((Villanueva et al., 1999), Figure 2b,c and Figure 3b,c). This was hypothesized to result from partial *INO* activity of the protein product of the mis-spliced *ino-4* mRNA. This product has a fifteen-nucleotide insertion that would result in insertion of five amino acids at Glu-147 in the translated protein and no other change in the reading frame (Villanueva et al., 1999). To determine whether the mutant protein has activity, we tested transgenic complementation of *ino-1* with a construct that produces the *ino-4*

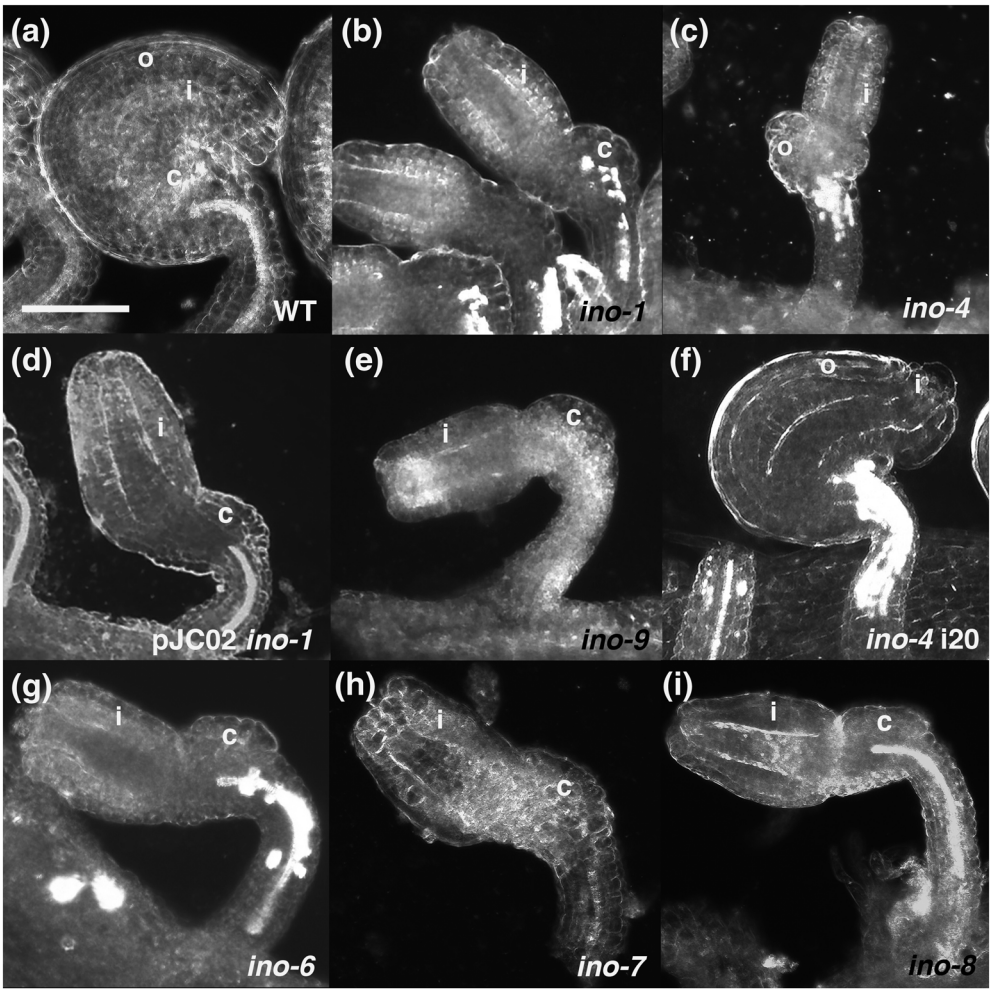

FIGURE 3 Dark field micrographs of Arabidopsis ovules. All ovules are from flowers at or just following anthesis and are oriented with the gynoapical side to the right. (a) Wild-type. (b) *ino-1*. (c) *ino-4*. (d) *ino-1* transformed with pJC02 transcribing *ino-4* mutant cDNA. (e) *ino-9*. (f) *ino-4 i20* double mutant. (g) *ino-6*. (h) *ino-7*. (i) *ino-8*. Bar in (a) is 50 µm in all panels. c, chalaza; i, inner integument; o, outer integument.

mutant protein. The wild-type cDNA was shown to be effective at complementing *ino-1*. A construct, pRJM33 (Villanueva et al., 1999), including 2.3 kb of *INO* 5′-flanking DNA, *INO* cDNA, and 2.0 kb of *INO* 3′-flanking DNA, led to the formation of fully wild-type ovules in 28 of 42 independently produced transgenic homozygous *ino-1* plants (Meister et al., 2005). When the wild-type *INO* cDNA was replaced in pRJM33 with the aberrantly spliced cDNA of *ino-4* and the resulting construct (pJC02) was introduced into plants, 29 of 29 independently transformed homozygous *ino-1* transgenics retained the *ino-1* ovule phenotype (Figure 2d and 3d). These results differ significantly ($p < .0001$, two-tailed Chi^2), demonstrating the failure of the *ino-4* cDNA sequence to complement the mutant and hence the failure of the extended *ino-4* protein to function.

3.2 | *ino-4* produces a small amount of wild-type *INO* mRNA

The finding that the *ino-4* aberrant mRNA/protein could not complement *ino-1* indicates there must be another source of active *INO* provided by the *ino-4* allele. RT-PCR analysis of mRNA from *ino-4* detected a prominent product of the expected size for the aberrant *ino-4* mRNA but also a smaller amount of a product that co-migrated with the product derived from mRNA from wild-type plants (Figure 4). To test if this product is properly spliced *INO* mRNA, we devised primers that cross the splice junction and would amplify only the properly spliced *INO* cDNA (Supporting information Table S1). We found that *ino-4* does produce wild-type mRNA, along with the mis-spliced *ino-4*-specific product (Figure 4).

3.3 | *INO* quantitatively affects ovule development

The effect of the apparent reduced level of functional *INO* in *ino-4* suggests that the quantity of *INO* differentially affects OI growth. A test of this hypothesis was serendipitously produced by our identification of a second-site suppressor of *ino-4* mutants. *Ino-4* plants produce small numbers of viable seeds, which served as a starting point for suppressor screening. We mutagenized *ino-4* seeds with fast neutrons and screened M2 plants for increased OI growth and increased fertility. One homozygous *ino-4* line, *i20*, had significantly more OI growth than *ino-4* single mutants, usually producing a nearly wild-type OI (Figure 2f and 3f). We evaluated the presence of wild-type *INO* mRNA in *ino-4* and *ino-4 i20*. *ino-4 i20* also produced both aberrant *ino-4* mRNA and wild-type mRNA (Figure 4), but both were at an apparently higher level than in *ino-4* (Figure 4).

Using segregating plants from a cross of *ino-4 i20* (in the Col background) to L*er*, we mapped the mutation in *i20* to the top of Chromosome 3. We used whole-genome sequencing to compare *ino-4 i20* sequence to the TAIR10 Col reference sequence (Lamesch et al., 2012). We found an apparent deletion within the mapped region on the basis of the absence of sequence reads (Figure 5a). This 57 bp deletion is between At3g10490 and At3g10500. Further work

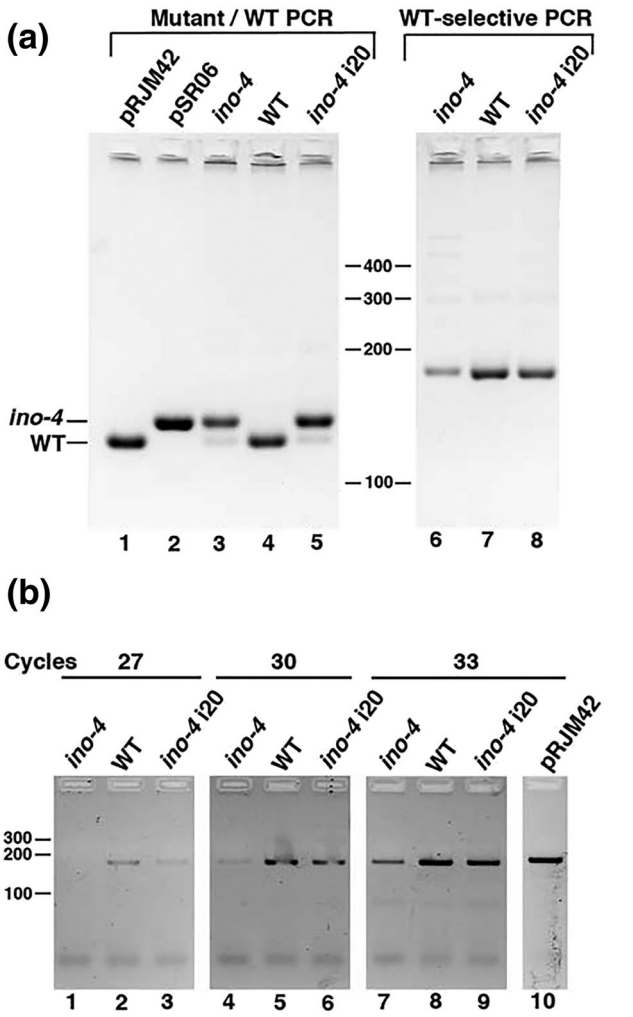

FIGURE 4 Reverse transcription polymerase chain reaction (PCR) detection of *INO* mRNA. (a) Lanes 1–5 show PCR products from primers flanking Intron 4 (*ino-4* FOR, *ino-4* REV) that will amplify cDNA from both mRNAs that utilized the wild-type splice site (WT) or the ectopic *ino-4* splice site (*ino-4*). Lanes 6–8 show products from primers that selectively amplify only cDNA from mRNA using the wild-type splice site due to one primer crossing the junction between Exons 4 and 5 (inoex45F2 with inoRTR1). Input DNA in lanes: (1) plasmid pRJM33, which includes the wild-type *INO* cDNA. (2) pSR06, which includes the cDNA to the aberrantly spliced *ino-4* cDNA. (3) and (6) cDNA to mRNA from *ino-4* flowers. (4) and (7) wild-type Col-0 flower cDNA. (5) and (8) cDNA to mRNA from *ino-4 i20* double mutant flowers. (b) PCR of cDNA from mRNA from flowers of the indicated plants or plasmid control (pRJM42) using primers selective for only the wild-type form of the *INO* mRNA. Samples were taken and evaluated following 27 cycles (Lanes 1–3), 30 cycles (Lanes 4–6), or 33 cycles (Lanes 7–10). Sizes of DNA markers are indicated in base pairs at the center (a) and left (b).

showed that there was a DNA insertion associated with the deletion. Individual reads that spanned this region were not present, and examination of the sequence reads at the borders of the deletion on Chromosome 3 showed that the reads paired with these reads were not aligned with Chromosome 3. Instead reads from one side of the deletion paired with reads mapped to a region on Chromosome 1, and

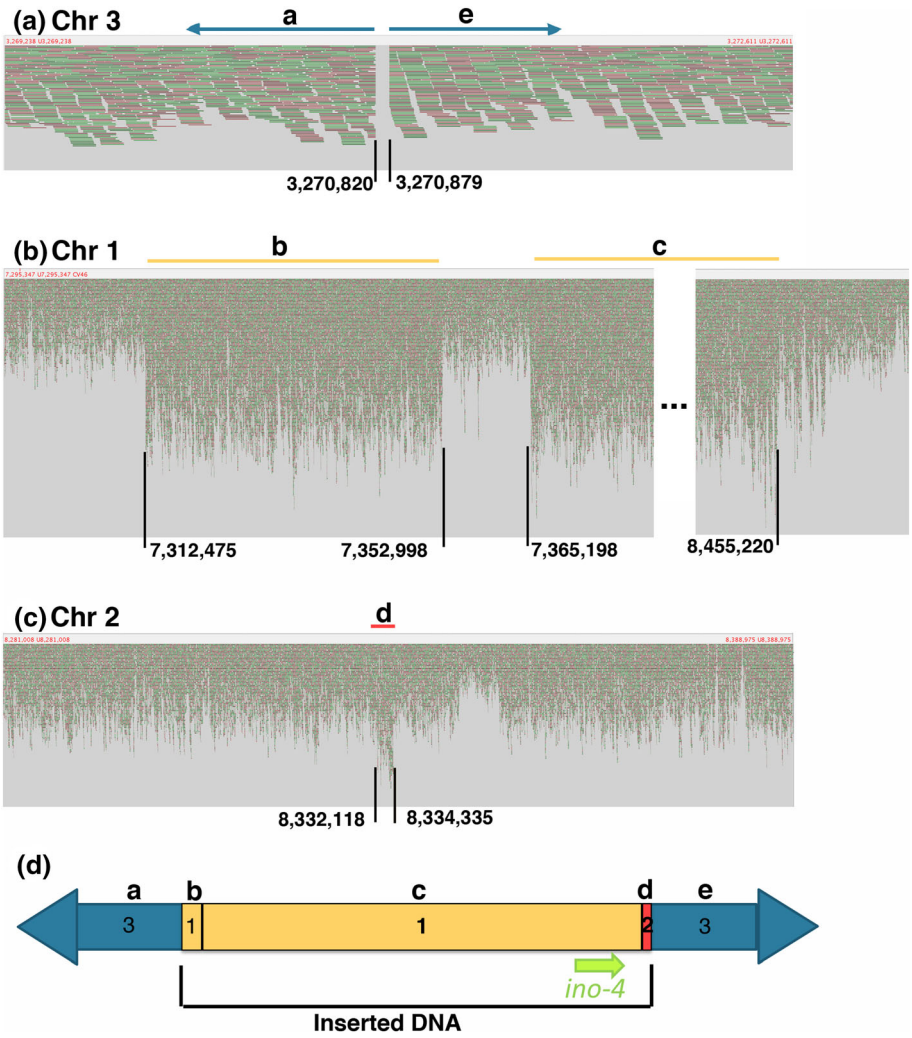

FIGURE 5 The structure of the insertion in the *i20* region. (a)–(c) Illumina sequence reads of homozygous *ino-4 i20* DNA aligned with wild-type Columbia Arabidopsis chromosomal regions as visualized in Tablet (Milne et al., 2013) software. Each ~100 base sequence read is shown as a colored line (appearing more as colored spots at the zoomed-out view in (b) and (c)) aligned below the corresponding sequence of the indicated Arabidopsis chromosome. (a) An absence of reads aligning with sequence between bases 3,270,821 and 3,270,878 of Chromosome 3 indicates deletion of this region, which is in the area within which *i20* was mapped. Reads immediately to the left and right side of the deletion were paired with locations on Chromosomes 1 and 2, respectively, indicating the presence of inserted DNA. (b) Two regions of Chromosome 1 show approximately twofold more reads than expected. Reads at 7,312,475 paired with reads on Chromosome 3 at Position 3,270,821. Reads at Position 8,455,220 paired with reads on Chromosome 2 at Position 8,332,118. (c) A region of Chromosome 2 also showed approximately twofold as many reads as an average region of the genome. Reads at 8,334,334 paired with reads on Chromosome 3 at Position 3,270,878. (d) Diagram of the structure of the insertion into Chromosome 3 of *i20* that is composed of regions of Chromosomes 1 and 2 (numbers indicate source chromosomes of the regions). Lower case letters at the top of the figure correspond to the chromosomal regions indicated by the same letters in panels (a)–(c). The location of the *ino-4* gene in an inserted Chromosome 1 region is indicated by the green arrow.

those at the other end of the deletion paired with reads mapped to a region on Chromosome 2. Examination of mapped reads in these regions of Chromosomes 1 and 2 showed an approximately twofold increase in depth of sequence reads, suggesting that these regions were duplicated in the genome. Two areas of Chromosome 1 showed this duplication: a ~40 kb region close to the *INO* locus and a second ~1.1 Mb region that included the *ino-4* sequence (Figure 5b). Similarly, this section of Chromosome 2 showed twofold more reads mapped over a 2.2 kb region (Figure 5c). The simplest explanation for this would be for regions of Chromosomes 1 and 2 to be duplicated and inserted into a small deletion on Chromosome 3. We used BLAST (Altschul et al., 1990) searches of our entire set of *i20* reads to identify individual reads that crossed the borders between the deletion site and the putative insertions and were able to find the expected numbers of such reads. Applying this method recursively, we were able to determine that a small region of Chromosome 2 and a larger portion of Chromosome 1, which included the *ino-4* locus, were duplicated and inserted into Chromosome 3 (Figure 5d and Supporting information Figure S1). Thus, the genome of *i20* included an extra copy of the *ino-4* locus on Chromosome 3. Using variable cycle counts in PCR, we

found that the level of wild-type mRNA was apparently higher in *ino-4 i20* than in *ino-4* but was still lower than in wild-type plants (Figure 4b). Thus, an increase in the level of wild-type mRNA in *ino-4 i20* over the minimal level present in *ino-4* induced increased OI growth and produced ovules closer in form to those of wild-type plants. This demonstrates that the role of *INO* activity in ovule development is not a binary switch, but rather, the activity quantitatively affects development of the OI.

The variable degree of OI formation in the different mutants showed corresponding differential effects on fertility and seed formation, and we quantitated these effects. The total numbers of ovules initiated in the different lines were similar, averaging between 26 and 33 per carpel (Supporting information Figure S2 and Supporting information Data S1). The fraction of ovules eventually forming seeds was high in the wild-type averaging 96% and 98% in Col and L*er*, respectively (Figure 6 and Supporting information Data S1). *ino-1* was largely infertile averaging only .3% of ovules setting seed, whereas *ino-4* was substantially more fertile with 12% of ovules forming seeds (Figure 6 and Supporting information Data S1). The addition of the *i20* translocation to *ino-4* restored a wild-type level of seed set with an average of 92% of ovules forming seeds (Figure 6 and Supporting information Data S1).

3.4 | Insertion mutant of *INO*

Because we had failed to isolate a clear null mutant of *INO* from chemically mutagenized material, we examined the set of available

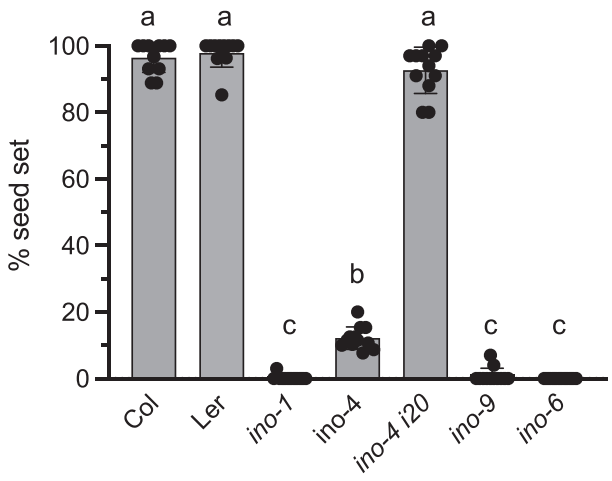

FIGURE 6 Percent of initiated ovules that go on to form seeds. Seeds and aborted ovules were counted in 12 carpels for each genotype. Percentage seed set was determined for each carpel by dividing the number of seeds formed by the total of seeds formed plus aborted ovules observed (X100). Black dots indicate actual determinations from each carpel; bars represent the mean of all of the determinations for that line; and whisker lines indicate the standard deviations of the means. Different letters (a, b, and c) indicate different sets of means that statistically differ from each other ($p < .01$) by Turkey's multiple comparison test.

Arabidopsis insertion mutants for insertions in the *INO* locus. We found only one line, SALK_0063818, which we designated *ino-9*. Sequencing of genomic DNA flanking the inserted T-DNA shows that the insertion is 162 bp 5′ of the translation start site of the *INO* coding region (Supporting information Figure S3). *ino-9* has a phenotype that precisely duplicates that of *ino-1* (Figure 2e and 3e). A seed set fraction of .4% was not statistically different from that of *ino-1* (Figure 6 and Supporting information Data S1). The insertion is between the regulatory region of the promoter and the coding sequence (Simon et al., 2012), apparently interrupting expression. However, like the *ino-1* mutation, this mutation does not preclude the possibility of formation of active *INO* protein as initiation of transcription induced within the insertion could still produce wild-type *INO* protein. As a result, we still did not have certainty that the *ino* null mutant phenotype had yet been observed.

3.5 | CRISPR-induced null *ino* mutants

In the absence of identifying a verified null mutant from random mutagenesis, we used CRISPR technology to induce deletion and insertion mutations in the coding region of *INO* that would cause frameshifts and preclude formation of the full *INO* protein. A plant transformation plasmid, pGD60, was constructed to produce the CAS9 protein and two guide RNAs directed to two locations in the coding region of *INO* and used to transform wild-type plants. The vector used included a cotyledon-expressed cassette producing GFP. This enabled simple isolation of M2 seeds, which had segregated out the CRISPR vector on the basis of the absence of GFP fluorescence (Aliaga-Franco et al., 2019). Multiple new *ino* mutant lines were isolated in the L*er* background, and three were chosen for complete characterization and designated *ino-6*, *−7*, and *−8* (Supporting information Figure S3). *ino-6* included a single-base deletion of a "T" residue at Position 80 (in the first exon) and a second mutation inserting a "T" residue after Position 883 (in Exon 5) of the coding region of *INO*. This would introduce a frameshift and cause mistranslation of the entire zinc-finger region and the first half of the *YABBY* domain (Figure S3). *ino-7* had an insertion of an "A" residue after Position 883 (in Exon 5) of the coding region, causing a frameshift of the second half of the *YABBY* domain (Villanueva et al., 1999) and all subsequent amino acids (Supporting information Figure S3). *ino-8* had a deletion of Bases 77 and 78 of the coding region (in Exon 1) of *INO*. This two-base deletion would cause a frameshift leading to mistranslation of all of the *INO* protein except the first 25 amino acids (Supporting information Figure S3). All three of these mutants eliminate regions of *INO* shown to be critical to its function (Meister et al., 2005) and hence are null mutations. Homozygous plants of all three mutants were indistinguishable from *ino-1* plants and wild-type plants in vegetative habit, and all three produced ovules that duplicated the *ino-1* and *ino-9* phenotypes (Figure 3). The seed set was examined in *ino-6* with no seeds observed, and this result was not statistically different from the extremely low seed set of *ino-1* and *ino-9* (Figure 6 and Supporting information Data S1). These results show that *ino-1* and *ino-9* are also

null mutants. Thus, the effects of *ino* complete loss-of-function mutants are confined to the OI of ovules, confirming the results of Vijayan et al. (2021).

4 | DISCUSSION

4.1 | *ino* null mutants

Until 2021, the two identified *ino* lesions had base substitutions that caused ectopic utilization of upstream splicing sites in *INO* pre-mRNA (Villanueva et al., 1999). Both retained the normal splice junctions and so had the potential for production of wild-type mRNA. This raised the possibility that null mutants had not been isolated. This failure to identify null mutants could result from such mutants being selected against due to pleiotropic effects. We first searched for null mutants in libraries of existing insertion mutants, but there, we found only a mutant with an insertion in the 5′-untranslated region. We could not say this was certainly null. We followed this by using CRISPR-based mutagenesis to produce frame-shift mutations in *INO* exons. Following completion of our mutagenesis, Vijayan et al. (2021) published work that included isolation of a putative null CRISPR-induced allele (*ino-5*). They reported the phenotype of *ino-5* as not significantly different from *ino-1*. Confirming this result, all three of our CRISPR-induced null mutants and also the insertion mutant duplicated the *ino-1* phenotypic effects. This indicates that *ino-1* also was null.

The null mutants all exhibited complete failure in formation of an OI ((Vijayan et al., 2021; Villanueva et al., 1999); Figure 1). All of the existing null mutants also exhibit only rare, sporadic formation of functional embryo sacs (Skinner & Gasser, 2009; Vijayan et al., 2021; Villanueva et al., 1999) and so rarely set seed (Figure 6 and Supporting information Data S1). In addition, the detailed imaging used by Vijayan et al. (2021) revealed subtle alterations in the formation of the nucellus and II. However, expression of *INO* has only been observed in the abaxial layer of the OI and never in these other affected cells and locations (Balasubramanian & Schneitz, 2000; Villanueva et al., 1999). Vijayan et al. (2021) hypothesize that absence of the OI would alter the hormonal environment during nucellar development. We note that allocation of nutritional resources would also be altered by absence of the OI, which would be expected to be a significant nutrient sink. Additionally, cell wall tension and other hydrostatic forces within the developing ovule would be altered by the absence of the confining OI, and such forces also have roles in morphogenesis (Green, 1996). On this basis, we concur with Vijayan et al. (2021) that the effects of *ino* mutations on the development of the II, nucellus, and embryo sac are most likely to be secondary effects of the absence of the OI and not direct effects of absence of active *INO* protein.

It is interesting to note that the only other plant in which an *ino* mutant has been identified to date was *Annona squamosa*, the sugar apple tree. In this *Thai seedless* (*Ts*) mutant, the embryo sac still formed in the majority of ovules despite the complete absence of an OI (Lora et al., 2011). In Arabidopsis, the tenuinucellate ovules have only a single nucellar cell layer surrounding the embryo sac, and this is sheathed in a thin two cell layer thick II (Robinson-Beers et al., 1992; Vijayan et al., 2021). In contrast, the crassinucellate ovules of *A. squamosa* are surrounded by a robust nucellus of at least four cell layers and an II comprising multiple cell layers at their micropylar end (Lora et al., 2011). Thus, even when the OI is absent, there is substantial maternal tissue surrounding the developing embryo sac that could insulate it from the effects of the absence of an OI. This could explain the further development of the embryo sac in the *ino* mutant in this species relative to Arabidopsis. The *ino* mutation in *A. squamosa* appears to be a complete deletion of the *INO* locus and hence is a null mutation (Lora et al., 2011). The absence of pleiotropic effects on other aspects of development in *A. squamosa* is thus consistent with the absence of pleiotropic effects now demonstrated for Arabidopsis *ino* null mutants.

4.2 | *INO* expression level correlates with the degree of OI growth

It had been previously hypothesized that the partial OI growth in *ino-4* resulted from a partially active protein produced from the mis-spliced but in-frame *ino-4* mRNA (Villanueva et al., 1999). The failure of a transgene transcribing the cDNA of the mis-spliced mRNA to induce any detectable OI growth demonstrated that this was not the case. The mis-spliced mRNA produces a protein with a five amino acid insertion in the *YABBY* domain (Villanueva et al., 1999), and our result shows that this protein is not active, supporting the importance of the integrity of this domain for function of the *INO YABBY* transcription factor. Instead, we were able to show that *ino-4* produces a small amount of properly spliced mRNA (Figure 4). That this low amount of *INO* mRNA is able to promote a minimal growth of the OI is an indication that *INO* quantitatively affects OI growth. Further evidence of this is provided by our isolation of a line with a translocated duplicate *ino-4* gene. As a result of the presence of this additional gene copy, this line has an increased level of wild-type mRNA over *ino-4* (Figure 4) and an apparent proportional increase in OI growth (Figure 2f and 3f) with a corresponding increase in seed set (Figure 6). Thus, *INO* is a direct quantitative regulator of OI growth rather than being a binary switch. This is consistent with the observed function of *INO* in wild-type plants. In situ hybridization and reporter transgene studies (Meister et al., 2002; Villanueva et al., 1999) show that *INO* is expressed at the highest level on the gynobasal side of the ovule where maximal OI growth takes place. The level of *INO* expression shows a progressive decrease toward the gynoapical side of the ovule, correlating with the decreased OI growth in this area that leads to the hood-like OI of wild-type ovules (Meister et al., 2002). In *superman* (*sup*) mutant ovules, there is increased OI growth on the gynoapical side of the ovule relative to wild-type (Gaiser et al., 1995). This correlates with an increase in *INO* expression in this region in such mutants (Meister et al., 2002). The correlation between developmental

evidence of quantitative effects of *INO* expression and our mutant studies linking quantity of *INO* expression and amount of OI growth provides robust evidence that the level of *INO* expression is a primary determinant of OI growth.

4.3 | Conclusion

The phenotypes of the null *ino* mutants demonstrate that this gene's role is specific to OI development in Arabidopsis. The specificity of the effects is mirrored in the confinement of *INO* expression to the outer (abaxial) layer of cells of the OI (Balasubramanian & Schneitz, 2002; Meister et al., 2002; Villanueva et al., 1999). This pattern of expression is conserved for *INO* orthologs among all examined angiosperms including other eudicots such as *Impatiens* and tomato (McAbee et al., 2005; Skinner et al., 2016), members of earlier diverging groups such as magnoliids in the *Annona* genus (Lora et al., 2011), and the very earliest diverging angiosperms including *Cabomba* and *Amborella* (Arnault et al., 2018; Yamada et al., 2003). Functional analysis of *INO* activity has been evaluated through virus-induced gene silencing in tobacco (Skinner et al., 2016) and through analysis of an *INO* deletion mutant in *Annona* (Lora et al., 2011) where effects similar to effects on Arabidopsis ovules were observed. Together, these results indicate that *INO* has had a primary role as a regulator of OI development from the inception of the angiosperms. The OI is a synapomorphy of angiosperms and is one of the defining features separating angiosperms from gymnospermous progenitors (Gasser & Skinner, 2019; Shi et al., 2021). Phylogenetic analysis of the *YABBY* gene family shows that the origin of the *INO* clade correlates with the origin of the angiosperms (Gasser & Skinner, 2019; Yamada et al., 2011). Thus, the origin of this critical or master gene for OI development (as shown by developmental and genetic analysis) may have been an essential step in the evolution of the OI and the origin of angiosperms (Gasser & Skinner, 2019; Shi et al., 2021).

AUTHOR CONTRIBUTIONS

Work was planned and conceived by Debra J. Skinner and Charles S. Gasser. Debra J. Skinner performed fast neutron mutagenesis and analysis. Charles S. Gasser and Trang Dang performed CRISPR mutagenesis and analysis. Charles S. Gasser wrote the manuscript with editing by Debra J. Skinner. All authors approved the manuscript.

ACKNOWLEDGMENTS

We thank Mily Ron and Anne Britt (Dept. of Plant Biology, University of California, Davis) for the gift of vectors and protocols for CRISPR mutagenesis; Judy Callis for aid in statistical analysis and advice on microscopy; and Selina Rodrigues, Jennifer Zonka, and George Day for excellent technical assistance.

CONFLICT OF INTEREST STATEMENT

The authors did not report any conflict of interest.

DATA AVAILABILITY STATEMENT

Newly derived plant lines have been deposited at the Arabidopsis Biological Resource Center at Ohio State, and other plant materials are available from the cited sources from which they were obtained. Raw genomic sequence data have been deposited in the NCBI SRA database under accession PRJNA866995.

ORCID

Charles S. Gasser https://orcid.org/0000-0001-5735-8175

REFERENCES

Aliaga-Franco, N., Zhang, C., Presa, S., Srivastava, A. K., Granell, A., Alabadi, D., Sadanandom, A., Blazquez, M. A., & Minguet, E. G. (2019). Identification of transgene-free CRISPR-edited plants of rice, tomato, and Arabidopsis by monitoring DsRED fluorescence in dry seeds. *Frontiers in Plant Science*, *10*, 1150. https://doi.org/10.3389/fpls.2019.01150

Alonso, J. M., Stepanova, A. N., Leisse, T. J., Kim, C. J., Chen, H., Shinn, P., Stevenson, D. K., Zimmerman, J., Barajas, P., Cheuk, R., Gadrinab, C., Heller, C., Jeske, A., Koesema, E., Meyers, C. C., Parker, H., Prednis, L., Ansari, Y., Choy, N., … Ecker, J. R. (2003). Genome-wide insertional mutagenesis of *Arabidopsis thaliana*. *Science*, *301*, 653–657. https://doi.org/10.1126/science.1086391

Altschul, S. F., Gish, W., Miller, W., Myers, E. W., & Lipman, D. J. (1990). Basic local alignment search tool. *Journal of Molecular Biology*, *215*, 403–410. https://doi.org/10.1016/S0022-2836(05)80360-2

Arnault, G., Vialette, A. C. M., Andres-Robin, A., Fogliani, B., Gateble, G., & Scutt, C. P. (2018). Evidence for the extensive conservation of mechanisms of ovule integument development since the most recent common ancestor of living angiosperms. *Frontiers in Plant Science*, *9*, 1352. https://doi.org/10.3389/fpls.2018.01352

Baker, S. C., Robinson-Beers, K., Villanueva, J. M., Gaiser, J. C., & Gasser, C. S. (1997). Interactions among genes regulating ovule development in *Arabidopsis thaliana*. *Genetics*, *145*, 1109–1124. https://doi.org/10.1093/genetics/145.4.1109

Balasubramanian, S., & Schneitz, K. (2000). *NOZZLE* regulates proximal-distal pattern formation, cell proliferation and early sporogenesis during ovule development in *Arabidopsis thaliana*. *Development*, *127*, 4227–4238. https://doi.org/10.1242/dev.127.19.4227

Balasubramanian, S., & Schneitz, K. (2002). NOZZLE links proximal-distal and adaxial-abaxial pattern formation during ovule development in *Arabidopsis thaliana*. *Development*, *129*, 4291–4300. https://doi.org/10.1242/dev.129.18.4291

Barro-Trastoy, D., Gómez, M. D., Tomero Feliciano, P., & Perez Amador, M. A. (2020). On the way to ovules: The hormonal regulation of ovule development. *Critical Reviews in Plant Sciences*, *39*, 431–456. https://doi.org/10.1080/07352689.2020.1820203

Clough, S. J., & Bent, A. F. (1998). Floral dip: A simplified method for *Agrobacterium*-mediated transformation of *Arabidopsis thaliana*. *The Plant Journal*, *16*, 735–743. https://doi.org/10.1046/j.1365-313x.1998.00343.x

Eshed, Y., Baum, S. F., Perea, J. V., & Bowman, J. L. (2001). Establishment of polarity in lateral organs of plants. *Current Biology*, *11*, 1251–1260. https://doi.org/10.1016/S0960-9822(01)00392-X

Gaiser, J. C., Robinson-Beers, K., & Gasser, C. S. (1995). The Arabidopsis SUPERMAN gene mediates asymmetric growth of the outer integument of ovules. *Plant Cell*, *7*, 333–345. https://doi.org/10.2307/3869855

Gasser, C. S., & Skinner, D. J. (2019). Development and evolution of the unique ovules of flowering plants. *Plant Development and Evolution*, *131*, 373–399. https://doi.org/10.1016/bs.ctdb.2018.10.007

Gleave, A. P. (1992). A versatile binary vector system with a T-DNA organisational structure conducive to efficient integration of cloned DNA into the plant genome. *Plant Molecular Biology*, *20*, 1203–1207. https://doi.org/10.1007/BF00028910

Green, P. B. (1996). Transductions to generate plant form and pattern: An essay on cause and effect. *Annals of Botany*, *78*, 269–281. https://doi.org/10.1006/anbo.1996.0121

Gross-Hardt, R., Kagi, C., Baumann, N., Moore, J. M., Baskar, R., Gagliano, W. B., Jurgens, G., & Grossniklaus, U. (2007). LACHESIS restricts gametic cell fate in the female gametophyte of Arabidopsis. *PLoS Biology*, *5*, e47. https://doi.org/10.1371/journal.pbio.0050047

Hou, X., Li, L., Peng, Z., Wei, B., Tang, S., Ding, M., Liu, J., Zhang, F., Zhao, Y., Gu, H., & Qu, L. J. (2010). A platform of high-density INDEL/CAPS markers for map-based cloning in Arabidopsis. *The Plant Journal*, *63*, 880–888. https://doi.org/10.1111/j.1365-313X.2010.04277.x

Jander, G., Norris, S. R., Rounsley, S. D., Bush, D. F., Levin, I. M., & Last, R. L. (2002). Arabidopsis map-based cloning in the post-genome era. *Plant Physiology*, *129*, 440–450. https://doi.org/10.1104/pp.003533

Kelley, D. R., Arreola, A., Gallagher, T. L., & Gasser, C. S. (2012). ETTIN (ARF3) physically interacts with KANADI proteins to form a functional complex essential for integument development and polarity determination in Arabidopsis. *Development*, *139*, 1105–1109. https://doi.org/10.1242/dev.067918

Kelley, D. R., Skinner, D. J., & Gasser, C. S. (2009). Roles of polarity determinants in ovule development. *The Plant Journal*, *57*, 1054–1064. https://doi.org/10.1111/j.1365-313X.2008.03752.x

Koncz, C., & Schell, J. (1986). The promoter of T_L-DNA gene 5 controls the tissue-specific expression of chimaeric genes carried by a novel type of *Agrobacterium* binary vector. *Molecular & General Genetics*, *204*, 383–396. https://doi.org/10.1007/BF00331014

Lamesch, P., Berardini, T. Z., Li, D., Swarbreck, D., Wilks, C., Sasidharan, R., Muller, R., Dreher, K., Alexander, D. L., Garcia-Hernandez, M., Karthikeyan, A. S., Lee, C. H., Nelson, W. D., Ploetz, L., Singh, S., Wensel, A., & Huala, E. (2012). The Arabidopsis information resource (TAIR): Improved gene annotation and new tools. *Nucleic Acids Research*, *40*, D1202–D1210. https://doi.org/10.1093/nar/gkr1090

Li, H. (2013). Aligning sequence reads, clone sequences and assembly contigs with BWA-MEM. arXiv **1303.3997**.

Lora, J., Hormaza, J. I., Herrero, M., & Gasser, C. S. (2011). Seedless fruits and the disruption of a conserved genetic pathway in angiosperm ovule development. *Proceedings of the National Academy of Sciences*, *108*, 5461–5465. https://doi.org/10.1073/pnas.1014514108

McAbee, J. M., Hill, T. A., Skinner, D. J., Izhaki, A., Hauser, B. A., Meister, R. J., Venugopala Reddy, G., Meyerowitz, E. M., Bowman, J. L., & Gasser, C. S. (2006). *ABERRANT TESTA SHAPE* encodes a KANADI family member, linking polarity determination to separation and growth of Arabidopsis ovule integuments. *The Plant Journal*, *46*, 522–531. https://doi.org/10.1111/j.1365-313X.2006.02717.x

McAbee, J. M., Kuzoff, R. K., & Gasser, C. S. (2005). Mechanisms of derived unitegmy among *impatiens* species. *Plant Cell*, *17*, 1674–1684. https://doi.org/10.1105/tpc.104.029207

Meister, R. J., Kotow, L. M., & Gasser, C. S. (2002). SUPERMAN attenuates positive INNER NO OUTER autoregulation to maintain polar development of Arabidopsis ovule outer integuments. *Development*, *129*, 4281–4289. https://doi.org/10.1242/dev.129.18.4281

Meister, R. J., Oldenhof, H., Bowman, J. L., & Gasser, C. S. (2005). Multiple protein regions contribute to differential activities of YABBY proteins in reproductive development. *Plant Physiology*, *137*, 651–662. https://doi.org/10.1104/pp.104.055368

Milne, I., Stephen, G., Bayer, M., Cock, P. J., Pritchard, L., Cardle, L., Shaw, P. D., & Marshall, D. (2013). Using tablet for visual exploration of second-generation sequencing data. *Briefings in Bioinformatics*, *14*, 193–202. https://doi.org/10.1093/bib/bbs012

Modrusan, Z., Reiser, L., Feldmann, K. A., Fischer, R. L., & Haughn, G. W. (1994). Homeotic transformation of ovules into carpel-like structures in Arabidopsis. *Plant Cell*, *6*, 333–349. https://doi.org/10.2307/3869754

Pauwels, L., De Clercq, R., Goossens, J., Inigo, S., Williams, C., Ron, M., Britt, A., & Goossens, A. (2018). A dual sgRNA approach for functional genomics in *Arabidopsis thaliana*. *G3 (Bethesda)*, *8*, 2603–2615. https://doi.org/10.1534/g3.118.200046

Pinyopich, A., Ditta, D. S., Savidge, B., Liljegren, S. J., Baumann, E., Wisman, E., & Yanofsky, M. F. (2003). Assessing the redundancy of MADS-box genes during carpel and ovule development. *Nature*, *424*, 85–88. https://doi.org/10.1038/nature01741

Plant, A. L., van Rooijen, G. J., Anderson, C. P., & Moloney, M. M. (1994). Regulation of an Arabidopsis oleosin gene promoter in transgenic *Brassica napus*. *Plant Molecular Biology*, *25*, 193–205. https://doi.org/10.1007/BF00023237

Ray, A., Robinson-Beers, K., Ray, S., Baker, S. C., Lang, J. D., Preuss, D., Milligan, S. B., & Gasser, C. S. (1994). The Arabidopsis floral homeotic gene *BELL* (*BEL1*) controls ovule development through negative regulation of *AGAMOUS* gene (*AG*). *Proceedings of the National Academy of Sciences*, *91*, 5761–5765. https://doi.org/10.1073/pnas.91.13.5761

Reiser, L., Modrusan, Z., Margossian, L., Samach, A., Ohad, N., Haughn, G. W., & Fischer, R. L. (1995). The *BELL1* gene encodes a homeodomain protein involved in pattern formation in the Arabidopsis ovule primordium. *Cell*, *83*, 735–742. https://doi.org/10.1016/0092-8674(95)90186-8

Robinson-Beers, K., Pruitt, R. E., & Gasser, C. S. (1992). Ovule development in wild-type Arabidopsis and two female-sterile mutants. *Plant Cell*, *4*, 1237–1249. https://doi.org/10.2307/3869410

Schneitz, K., Hulskamp, M., & Pruitt, R. E. (1995). Wild-type ovule development in *Arabidopsis thaliana*: A light microscope study of cleared whole-mount tissue. *The Plant Journal*, *7*, 731–749. https://doi.org/10.1046/j.1365-313X.1995.07050731.x

Shi, G., Herrera, F., Herendeen, P. S., Clark, E. G., & Crane, P. R. (2021). Mesozoic cupules and the origin of the angiosperm second integument. *Nature*, *594*, 223–226. https://doi.org/10.1038/s41586-021-03598-w

Sieber, P., Gheyselinck, J., Gross-Hardt, R., Laux, T., Grossniklaus, U., & Schneitz, K. (2004). Pattern formation during early ovule development in *Arabidopsis thaliana*. *Developmental Biology*, *273*, 321–334. https://doi.org/10.1016/j.ydbio.2004.05.037

Simon, M. K., Williams, L. A., Brady-Passerini, K., Brown, R. H., & Gasser, C. S. (2012). Positive- and negative-acting regulatory elements contribute to the tissue-specific expression of *INNER NO OUTER*, a YABBY-type transcription factor gene in Arabidopsis. *BMC Plant Biology*, *12*, 214. https://doi.org/10.1186/1471-2229-12-214

Skinner, D. J., Brown, R. H., Kuzoff, R. K., & Gasser, C. S. (2016). Conservation of the role of INNER NO OUTER in development of unitegmic ovules of the Solanaceae despite a divergence in protein function. *BMC Plant Biology*, *16*, 143. https://doi.org/10.1186/s12870-016-0835-z

Skinner, D. J., & Gasser, C. S. (2009). Expression-based discovery of candidate ovule development regulators through transcriptional profiling of ovule mutants. *BMC Plant Biology*, *9*, 29. https://doi.org/10.1186/1471-2229-9-29

Vijayan, A., Tofanelli, R., Strauss, S., Cerrone, L., Wolny, A., Strohmeier, J., Kreshuk, A., Hamprecht, F. A., Smith, R. S., & Schneitz, K. (2021). A digital 3D reference atlas reveals cellular growth patterns shaping the Arabidopsis ovule. *eLife*, *10*, e63262. https://doi.org/10.7554/eLife.63262

Villanueva, J. M., Broadhvest, J., Hauser, B. A., Meister, R. J., Schneitz, K., & Gasser, C. S. (1999). *INNER NO OUTER* regulates abaxial-adaxial patterning in Arabidopsis ovules. *Genes & Development*, *13*, 3160–3169. https://doi.org/10.1101/gad.13.23.3160

Yamada, T., Ito, M., & Kato, M. (2003). Expression pattern of *INNER NO OUTER* homologue in *Nymphaea* (water lily family, Nymphaeaceae). *Development Genes and Evolution*, *213*, 510–513. https://doi.org/10.1007/s00427-003-0350-8

Yamada, T., Yokota, S., Hirayama, Y., Imaichi, R., Kato, M., & Gasser, C. S. (2011). Ancestral expression patterns and evolutionary diversification of YABBY genes in angiosperms. *The Plant Journal*, *67*, 26–36. https://doi.org/10.1111/j.1365-313X.2011.04570.x

SUPPORTING INFORMATION

Additional supporting information can be found online in the Supporting Information section at the end of this article.

How to cite this article: Skinner, D. J., Dang, T., & Gasser, C. S. (2023). The Arabidopsis *INNER NO OUTER* (*INO*) gene acts exclusively and quantitatively in regulation of ovule outer integument development. *Plant Direct*, *7*(2), e485. https://doi.org/10.1002/pld3.485